



INSTITUT NATIONAL POLYTECHNIQUE DE TOULOUSE

MASTER RECHERCHE DET

YEAR 2015

Study of spark plug ignition

Author:
Rodrigo Méndez Rojano

Supervisors:
Bénédicte Cuenot
Olivier Vermorel
Dario Maestro



June 2015

ABSTRACT

A coupling strategy between a magneto-hydrodynamics (MHD) plasma simulation and a direct numerical simulation of a non reactive and a reactive flow is presented for spark ignition. Ignition is a key factor for reducing pollutants and for extending the working limits of internal combustion engines. More generally, successful ignition and combustion propagation are generic problems in the development of many types of engines.

The aim of the present coupling strategy is to take into account the effects of the plasma physics which control the early stages of the spark electric discharge. Non reactive simulations initialized with an instantaneous solution from MHD with chemical equilibrium, taken at various stages after sparking, showed similar results between the two types of simulation. In particular, the shock propagation velocity was recovered. From these results it can be concluded that the effects on the flow of the magnetic field induced by the plasma can be neglected after $0.525[\mu s]$.

A reactive simulation of a CH_4/AIR mixture was then performed after replacing air by burnt and fresh gases in the instantaneous solutions of the MHD simulation. A reduced, globally fitted chemical scheme was used. The results proved the capability of the code aVBP to start combustion in the high pressure and temperature conditions imposed by the plasma.

Une stratégie de couplage entre une simulation magnéto-hydrodynamique de plasma (MHD) et une simulation numérique directe d'un écoulement réactif et non réactif, est présentée dans le contexte de l'allumage par bougie. L'allumage est un facteur clé pour la réduction des polluants et pour étendre les limites de fonctionnement de moteurs à combustion interne. Le succès de l'allumage ainsi que la propagation de la combustion sont des problématiques classiques dans le développement de nombreux moteurs.

L'objectif de la stratégie de couplage présentée ici est de prendre en compte les effets de la physique du plasma qui contrôlent les premiers instants d'allumage. Les simulations non réactives initialisées avec une solution instantanée de MHD à l'équilibre chimique prise à différents instants après le claquage de la bougie montrent des résultats similaires entre les deux types de simulation. En particulier la même vitesse de propagation du choc est retrouvée. Ces résultats permettent de conclure que les effets du champ magnétique dûs au plasma sont négligeables après $0,525[\mu s]$.

Une simulation réactive d'un mélange CH_4/AIR a ensuite été réalisée en remplaçant l'air par des gaz brûlés et des gaz frais dans les solutions de la simulation MHD. Une chimie réduite à deux étapes a été utilisée. Les résultats montrent la capacité du code AVBP à démarrer la combustion dans des conditions de haute pression et haute température imposées par le plasma.

Contents

Contents	ii
1 Introduction	1
1.1 Host Enterprise	1
1.2 Project Description	2
2 Literature review	4
2.1 Blast wave	5
2.2 Plasma effect	7
3 AVBP & Direct numerical simulations equations	9
3.1 Direct numerical simulation	9
3.1.1 Set of Equations for DNS	10
3.2 Implementation of the equations in AVBP	11
3.2.1 Thermodynamic variables	11
3.2.2 Gas constant r and heat capacities	12
3.2.3 Species diffusion flux	12
3.2.4 Heat flux vector	13
3.2.5 Transport coefficients	13
3.2.6 Kinetics	14
4 DNS of 2D spark plug ignition	16
4.1 Set up and coupling	16
4.1.1 FLUENT (MHD) and AVBP coupling	16
4.1.2 FLUENT (MHD) and AVBP simulations	19
4.2 Non reactive simulations	20
4.3 Reactive simulations	28
5 Conclusions	33
Bibliography	35

Chapter 1

Introduction

1.1 Host Enterprise

CERFACS stands for "European Center for Research and Advanced Training in Scientific Computation"¹. It is a private, non-commercial research center, supported by seven shareholders being industry or public institutions (Meteo-France, CNES, EDF, Airbus, Safran, Total, ONERA). The main research areas at CERFACS are numerical simulation and algorithmic solutions for large scientific and technological problems, in the context of High Performance Computing (HPC). Applications cover a wide range of problems, from fundamental research to industrial systems. HPC capabilities are offered from an indoor capacity of 75 Tflop/s, and from the access to external computers in the framework of GENCI or PRACE.

The research groups at CERFACS are divided in:

- Computational Fluid Dynamics (CFD)
- Climate modelling and global change
- Aviation and Environment
- Parallel algorithms

These groups are composed from interdisciplinary teams, both for research and advanced training that are comprised of physicists, applied mathematicians, numerical analysts, and software engineers. Within these teams several codes and tools are constantly being developed. The current study is performed in the CFD team, using the AVBP code for reacting turbulent flows developed by CERFACS and IFPEN².

¹in french : Centre Européen de Recherche et de Formation Avancée en Calcul Scientifique

²Institut Français de Pétrole Energies Nouvelles

This master project is part of the FAMAC³ ANR project, gathering various laboratories (CORIA, EM2C, LAPLACE), research institutes (CERFACS, IFPEN) and industry (CONTINENTAL) and started in 2012. The objective is to better understand the early stages of spark ignition in order to propose innovative solutions for better performances.

1.2 Project Description

The study of ignition systems for internal combustion engines has a great importance for the design and development of new engines. A constant design concern, always present in new developments, is the difficulty to ignite in an economic (ie; with minimum energy) and reliable way. In addition, new engines will need to extend their operation limits to reach the future regulations on fuel consumption and pollutant emissions, which will make ignition even more difficult to achieve and control. As an example, European regulations on CO_2 emissions for road transportation vehicles [1] state that by 2021 the fleet average to be achieved by all new cars is 95 grams of CO_2 per kilometer.

In this context, several concepts have been proposed such as downsizing or pulsated plasma ignition [2], [3], [4]. Downsizing has already proven to be a good candidate to reduce CO_2 emissions but raises new problems linked to the control of combustion initiation and propagation, leading to auto-ignition, engine knock or even failed ignition [5].

The FAMAC project studies ignition fundamentals for internal combustion engines, to understand the physics of the electric arc. It integrates different levels of modeling, simulation and experiments for cross-validation and development of innovative solutions.

In Internal Combustion engines, several ignition systems are found, like spark plugs, lasers or glow-plugs. The present project focuses on spark plugs, where a discharge electric current delivered in the combustion chamber ignites the fuel/air mixture. The electrical discharge is characterized by the apparition of a plasma followed by a blast wave. A look at the literature shows that studies that take into account all the involved physics in a spark ignition process are very difficult: ionization[6], plasma kernel growth, blast wave effect [7], geometry, energy distribution, discharge types[8], or turbulence [9]) are all important phenomena that need to be described. Simplified models like 0D thermodynamic models or simple chemistry 2D models were developed but they do not give

³Fondamentaux d'Allumage pour Moteurs à Allumage Commandé

clear explanations. Spark ignition remains therefore a relevant and crucial current research topic.

To link the spark discharge to the start of a flame, several steps and effect must be described:

- From the plasma to the combustion mixture and chemistry.
- The start of the flame and the associated chemical model.
- The impact of the electrodes geometry and heat transfers.

Over the last two years work has been done at CERFACS in order to account the high temperatures and pressures reached in the plasma. In [10], the thermodynamics and transport properties were validated for very high temperatures. A complex chemical scheme with 72 reactions was then implemented and compared to a simpler scheme. Additionally Maestro et.al. [11] performed a full 3D ignition simulation with a real electrode geometry [12]. Good agreement was found between the AVBP simulation, the model of Kravchik et.al. and the experimental results from [8].

The objective of the present study is to evaluate the impact of magnetic/electric field on the ignition process after the spark discharge. To do so, results from a non reactive plasma model (MHD)⁴ are compared to a direct numerical simulation of both non reactive and reactive flows without the magnetic/electric field. The Fluent (MHD) simulation was performed by the Laplace laboratory, where the first instants of the ignition process $t < 3.5[\mu s]$ were computed. Then an instantaneous solution from the Fluent (MHD) simulation was taken as initial solution for the reactive and non reactive AVBP computations.

⁴Magneto-hydrodynamics, combination of the Navier-Stokes equations of fluid dynamics and Maxwell's equations of electromagnetism

Chapter 2

Literature review

The physics behind the spark ignition phenomena are not fully understood. Even for a quiescent mixture a complete theory has not been yet established and no one has been able to correlate accurately the combustion outcome to the spark parameters in a controllable way. A variety of theories have been developed [13] - [14], identifying several aspects that need to be taken into account:

- Characteristics of the spark discharge, time dependency of the electrical signal
- Chemical kinetics at the plasma channel and after the spark in the flame kernel [15]
- Energy distribution in the plasma kernel
- Influence of the mixture composition and fuel type
- Aerodynamic flow induced by the expanding spark kernel

Maly et.al. [8] presented an experimental work in which they observed the electrical characteristics of the spark signal. High pressure low-current discharges were observed and three main types of discharge were identified: the break down, glow and arc discharges. Results showed that a part of the energy was lost by dissipation in the anode and cathode, whereas the rest of the energy was available and responsible for the flame initiation process.

To better understand how spark flames propagate, Kravchick et.al. [12] performed a 2D direct numerical simulation of the experimental set up from [8] with a quiescent mixture of CH_4/AIR . Kravchick started the simulation after the breakdown phase and supposed a plasma channel with uniform properties (pressure and temperature). Results

showed that during the phase of kernel growth 27% of the energy was transferred to the flame, while heat losses concentrated in conduction within the electrodes by 70% and in thermal radiation by 3% of the electrical energy. Figure 2.1 illustrates the evolution of heat losses in time.

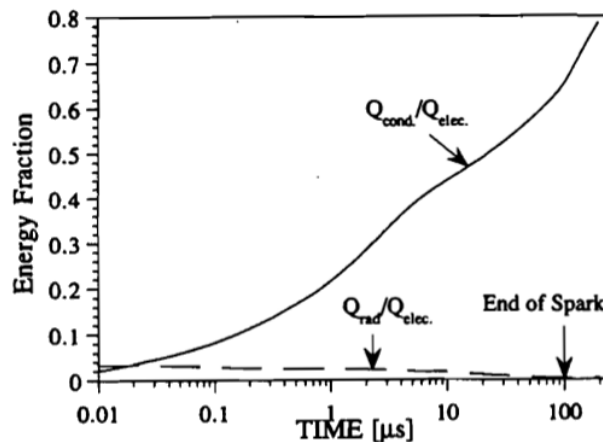


FIGURE 2.1: Evolution of heat losses, conduction Q_{cond} , radiation Q_{rad} . The electrical energy supply corresponds to $E = 2.8[mJ]$

At the early stage of ignition the laminar flow governs the expansion of the flame kernel. Turbulent effects appear later in the propagation of the flame in the chamber volume, which is a longer process and is out of the scope of this work.

2.1 Blast wave

After the spark discharge a shock wave is observed, which occurs faster than the chemistry. A fundamental theory of blast waves is the classical similar solution of Taylor [16], which considers that a finite amount of energy is suddenly released in a concentrated form. Taylor proposed that after the energy deposit, a spherical shock wave is propagated outwards, having a radius R function of time t and depending on the energy deposit E as:

$$R = S(\gamma)t^{2/5}E^{1/5}\rho_0^{-1/5} \quad (2.1)$$

where S is function of γ the ratio of the specific heats of air. Taylor proposed the following dimensionless functions:

$$\eta = \frac{r}{R} \quad (2.2)$$

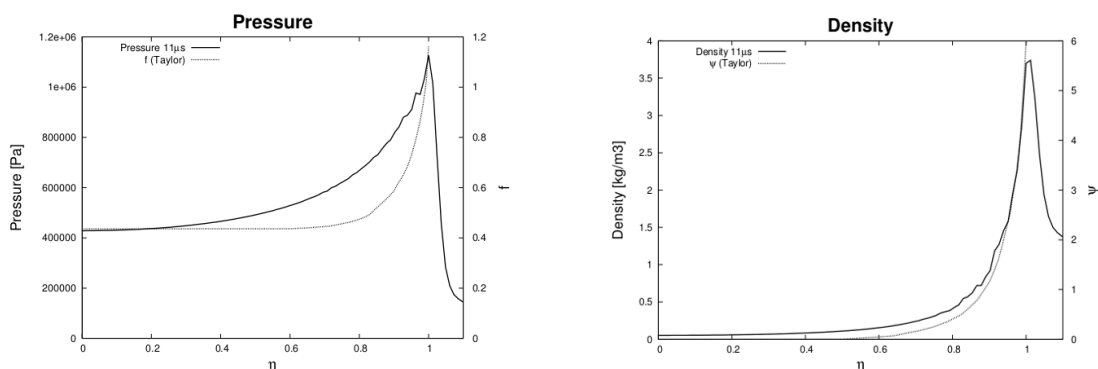
$$f = f_1 \frac{a^2}{A^2} \quad (2.3)$$

$$\psi = \frac{\rho}{\rho_0} \quad (2.4)$$

$$\phi = \frac{\phi_1}{A} \quad (2.5)$$

This relations can be reduced so that η , f , ϕ , ψ depend only on γ . Taylor resolved the problem for $\gamma = 1.4$ and varied η from $\eta = 1$ to $\eta = 0.5$. This analytical exact solution can be used as a reference for numerical simulations.

In order to confront the AVBP code with a spark ignition problem, Maestro [11] performed a 1D simulation of a deposit of Energy in a non-reactive mixture. The energy deposit is $E = 0.75[\frac{MJ}{m^2}]$ with a radius of 15 [mm], and the duration of energy deposition is 10[μs]. Following Taylor, $f \propto P$, $\phi \propto U$ and $\phi \propto density$. Figure 2.2 to Figure 2.3 show a comparison between the numerical solution from Taylor and the solution from AVBP to the 1D problem.



a) Pressure [Pa] in function of η

b) Density $\frac{Kg}{m^3}$ in function of η

FIGURE 2.2: 1D shock after energy deposit. Continuous line corresponds to the AVBP calculation, dot line corresponds to the Taylor analytical solution

In the same work of Maestro [11] a DNS with a similar configuration as in [12] was performed. Figure 2.4 shows a comparison of the pressure wave development between the experimental results from [8] and both numerical simulations. We can observed that for early stages of the pressure wave development the results from AVBP have a better agreement than the ones from Kravchick, after 10[μs] both simulations present almost

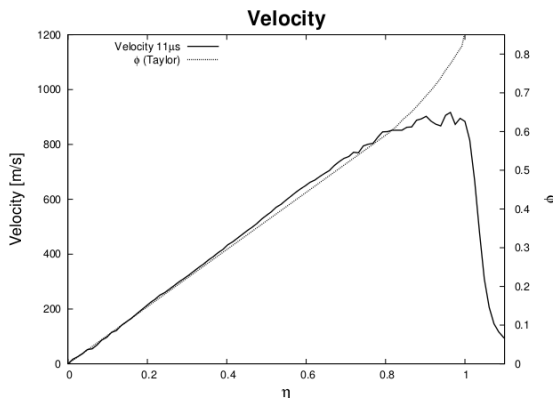
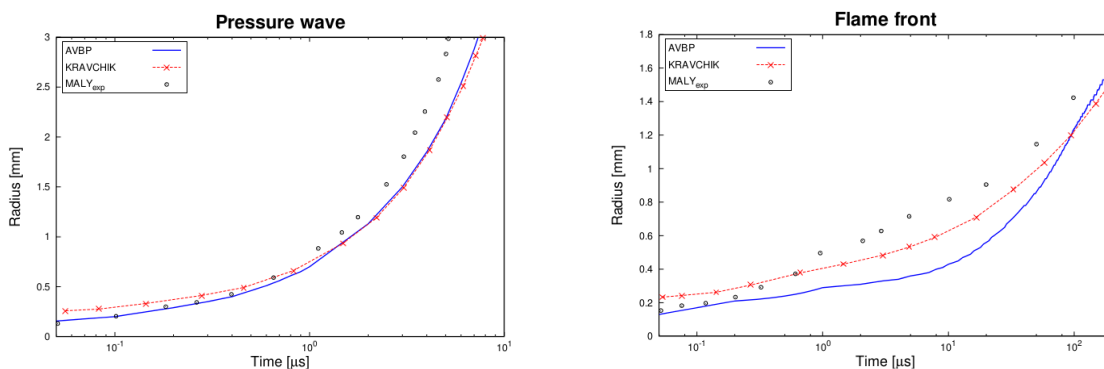


FIGURE 2.3: 1D shock after energy deposit. Velocity evolution in function of η . Continuous line corresponds to the AVBP calculation, dot line corresponds to the analytical solution of Taylor

the same behavior.



a) Pressure wave radius [m] in function of time

b) Flame front radius [m] in function of time

FIGURE 2.4: 3D ignition simulation. Blue continuous line corresponds to the AVBP calculation, red dashed line with crosses corresponds to the solution of Kravchik and symbols are for experiment values.

2.2 Plasma effect

Most plasma studies focused on nanosecond electric arcs. In this type of arcs, the effect of the plasma on the combustion is the formation of radicals that can facilitate ignition. In [17] a strategy to take into account the effect of the plasma in a mixture containing CH_4 is presented. Firstly the Boltzmann equation for electrons in weakly ionized gases in uniform electric fields is resolved numerically with the software Bolsig+ [18]. The numerical solution of the Boltzmann equation gives several outputs like the reaction rate of species. The most representative species (from a thermodynamic point of view) are

preserved to continue a reactive simulation using the CANTERA software. In Figure 2.2 the final output of CANTERA is presented. This method was also used in CH_6 to C_5H_{12} containing mixtures [15]. The authors conclude that by using this method an ignition time delay can be found.

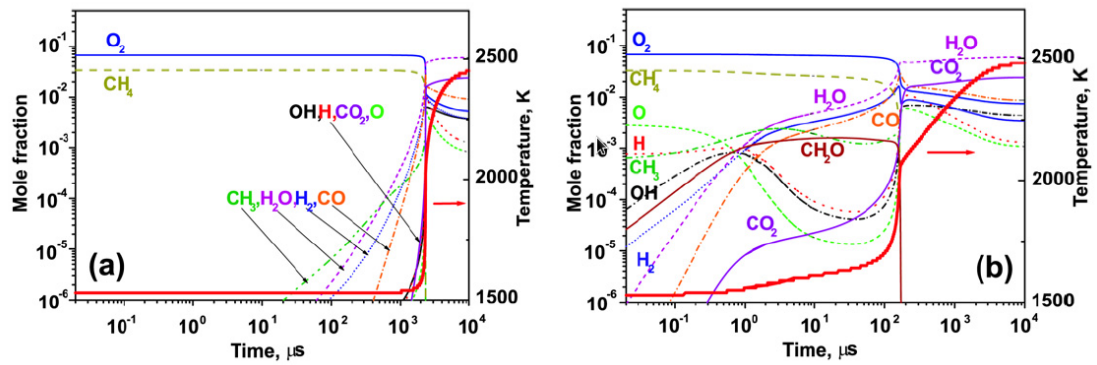


FIGURE 2.5: Evolution in time of composition, in CH_4 containing mixture

Chapter 3

AVBP & Direct numerical simulations equations

In this chapter the governing equations for the Direct Numerical Simulations (DNS) with AVBP will be presented. How the high temperature and high pressure are taken into account in the code for the particular case of ignition with an electric discharge is also described.

The AVBP code is a parallel CFD ¹ unstructured solver, it is capable of handling grids of any cell type in order to solve the three-dimensional compressible, reactive conservation equations. AVBP is widely used to perform LES² of reacting flows.

3.1 Direct numerical simulation

DNS consists of fully solving the complete set of compressible Navier-Stokes equations, without any type of model for the turbulence that is full resolved until the Kolmogorov's scale. It is important to say that DNS is a really accurate and expensive tool, suitable for small computational domains and academic cases. DNS is a good candidate for the present study because of the small computational domain (spark diameter is $150[\mu m]$). Also, as mentioned in chapter 2, the development of the flame kernel is dictated by the laminar flow surrounding the kernel, for this reason no turbulence model should not be used at the early stages of ignition.

¹Computational Fluid Dynamics

²Large eddy simulations

3.1.1 Set of Equations for DNS

The set of conservative equations to solve reacting flows are presented here as in [19], the index notation is adopted (Einstein's rule of summation). Note however that the index k refers to the k^{th} species.

$$\frac{\partial \rho}{\partial t} + \frac{\partial \rho u_i}{\partial x_i} = 0 \quad (3.1)$$

$$\frac{\partial \rho Y_k}{\partial t} + \frac{\partial}{\partial x_i} (\rho (u_i + V_{k,i}) Y_k) = \dot{\omega}_k \quad (3.2)$$

$$\frac{\partial}{\partial t} \rho u_j + \frac{\partial}{\partial x_i} \rho u_i u_j = -\frac{\partial p}{\partial x_j} + \frac{\partial \tau_{ij}}{\partial x_i} + \rho \sum_{k=1}^N Y_k f_{k,j} \quad (3.3)$$

$$\frac{\partial \rho E}{\partial t} + \frac{\partial}{\partial x_i} \rho u_i E = \dot{\omega}_T - \frac{\partial q_i}{\partial x_i} + \frac{\partial}{\partial x_j} (\sigma_{ij} u_i) + \dot{Q} + \rho \sum_{k=1}^N Y_k f_{k,i} (u_i + V_{k,i}) \quad (3.4)$$

Eqs. [3.1- 3.4], are mass, species, momentum and energy conservation equations respectively where:

- ρ : density
- u_i : velocity vector
- E : total mass energy
- Y_k : mass fraction from species k for $k = 1$ to $N - 1$
- N : number of species
- $V_{k,i}$ diffusion velocity of species k
- $\dot{\omega}_k$ reaction rate of species k
- p : pressure
- $\tau_{ij} = 2\mu(S_{ij} - \frac{1}{3}\delta_{ij}S_{ll})$: viscous tensor where $S_{ij} = \frac{1}{2} \left(\frac{\partial u_j}{\partial x_i} + \frac{\partial u_i}{\partial x_j} \right)$
- $\dot{\omega}_T$: heat release due to combustion
- \dot{Q} : external heat source term
- f_k measures the volume forces applied on species k .

For a deeper description of each term please refer to [19]

3.2 Implementation of the equations in AVBP

The development of the code AVBP started in 1993, first in Fortran 70 with some sub-routines in C for the dynamic allocation of memory. Nowadays the code has been upgraded to Fortran 90/95. In this section some terms of the DNS equations are presented in the same form in which they are implemented in AVBP.

3.2.1 Thermodynamic variables

In AVBP the standard thermodynamic reference state is $P_0 = 1[\text{bar}]$ and $T_0 = 0[\text{K}]$. The sensible mass enthalpies ($h_{s,k}$) and entropies (s_k) for each species are tabulated for 501 values of the temperature in a range of 0K to 50000 K with a step of 100K. Finally the variables are calculated as follow:

$$h_{s,k}(T_i) = \int_{T_0=0\text{K}}^{T_i} C_{p,k} dT = \frac{h_{s,k}^m(T_i) - h_{s,k}^m(T_0)}{W_k}, \quad (3.5)$$

and,

$$s_k(T_i) = \frac{s_k^m(T_i) - s_k^m(T_0)}{W_k}, \quad (3.6)$$

The superscript m corresponds to molar values. The tabulated values for $h_{s,k}(T_i)$ and $s_k(T_i)$ can be found in the NASA [20],[21] or CHEMKIN [22] tables. For the case of an energy deposition with a spark, the temperature can rise up to 45000 K. The nine coefficients approach from NASA allows to extrapolate the tables until 20000 K with relative good accuracy.

Incidentally, we must not forget that the mass heat capacities at constant pressure $c_{p,k}$ and volume $c_{v,k}$ are supposed constant between T_i and T_{i+1} . Therefore the sensible energy varies continuously with the temperature and is obtained by means of linear interpolation:

$$e_{s,k}(T) = e_{s,k}(T_i) + (T - T_i) \frac{e_{s,k}(T_{i+1}) - e_{s,k}(T_i)}{T_{i+1} - T_i} \quad (3.7)$$

The sensible energy and enthalpy are finally compute as:

$$\rho e_s = \sum_{k=1}^N \rho_k e_{s,k} = \rho \sum_{k=1}^N Y_k e_{s,k} \quad (3.8)$$

$$\rho h_s = \sum_{k=1}^N \rho_k h_{s,k} = \rho \sum_{k=1}^N Y_k h_{s,k} \quad (3.9)$$

3.2.2 Gas constant r and heat capacities

The gas constant r and the heat capacities of the gas mixture depend on the local gas composition and they read as follows:

$$r = \frac{R}{W} = \sum_{k=1}^N \frac{Y_k}{W_k} R = \sum_{k=1}^N Y_k r_k, \quad (3.10)$$

where W is the mean molecular weight and $R = 8.3143[\frac{J}{molK}]$ is the universal gas constant.

$$\frac{1}{W} = \sum_{k=1}^N \frac{Y_k}{W_k} \quad (3.11)$$

$$C_p = \sum_{k=1}^N Y_k C_{p,k} \quad (3.12)$$

$$C_v = \sum_{k=1}^N Y_k C_{v,k} \quad (3.13)$$

3.2.3 Species diffusion flux

Eq. 3.2 can also be written:

$$\frac{\partial \rho_k}{\partial t} + \frac{\partial}{\partial x_j} (\rho_k u_j) = -\frac{\partial}{\partial x_j} [J_{j,k}] + \dot{\omega}_k \quad (3.14)$$

For multi-species flows the total mass is conserved and so:

$$\sum_{k=1}^N Y_k V_i^k = 0, \quad (3.15)$$

where V_i^k is the diffusion velocity of species k . Using the Hirschfelder Curtis approximation:

$$X_k V_i^k = -D_k \frac{\partial X_k}{\partial x_i}, \quad (3.16)$$

where X_k is the molar fraction of species k and is defined as: $X_k = \frac{Y_k W}{W_k}$, in order to ensure global mass conservation Eq. 3.15 a diffusion velocity V_i^c is added.

$$V_i^c = \sum_{k=1}^N D_k \frac{W_k}{W} \frac{\partial X_k}{\partial x_i} \quad (3.17)$$

Finally the diffusive species flux reads:

$$J_{i,k} = -\rho \left(D_k \frac{W_k}{W} \frac{\partial X_k}{\partial x_i} - Y_k V_i^c \right), \quad (3.18)$$

with D_k as the diffusion coefficients for each species k .

3.2.4 Heat flux vector

In Eq. 3.4 the heat flux contains an additional term linked to the multi-species mixture. It is due to the heat transported by species diffusion and writes:

$$q_i = -\lambda \frac{\partial T}{\partial x_i} - \rho \sum_{k=1}^N \left(D_k \frac{W_k}{W} \frac{\partial X_k}{\partial x_i} - Y_k V_i^c \right) h_{s,k} = -\lambda \frac{\delta T}{\delta x_i} + \sum_{k=1}^N J_{i,k} h_{s,k}, \quad (3.19)$$

where the first term is the heat conduction coefficient λ and the second term is the flux due to species diffusion.

3.2.5 Transport coefficients

In AVBP there are several ways to compute the molecular viscosity μ . The Sutherland law and the Power law are used most often. The Sutherland law assumes the molecular viscosity to be independent of the gas composition and it is written as follows:

$$\mu = c_1 \frac{T^{3/2}}{T + c_2} \frac{T_{ref} + c_2}{T_{ref}^{3/2}} \quad (3.20)$$

where T_{ref} , c_1 , and c_2 depend on the mixture. The power law is computed as follow:

$$\mu = c_1 \left(\frac{T}{T_{ref}} \right)^b \quad (3.21)$$

For high temperatures $T > 3000k$, according to the studies performed by [?], the molecular viscosity has a particular behavior which is strongly dependent on the temperature and pressure. The implementation within AVBP was done in [?] and validated with a 1D temperature gradient of 300 to 45000 [K] with air and $P = 101325.0[Pa]$. The results are shown in Figure ??.

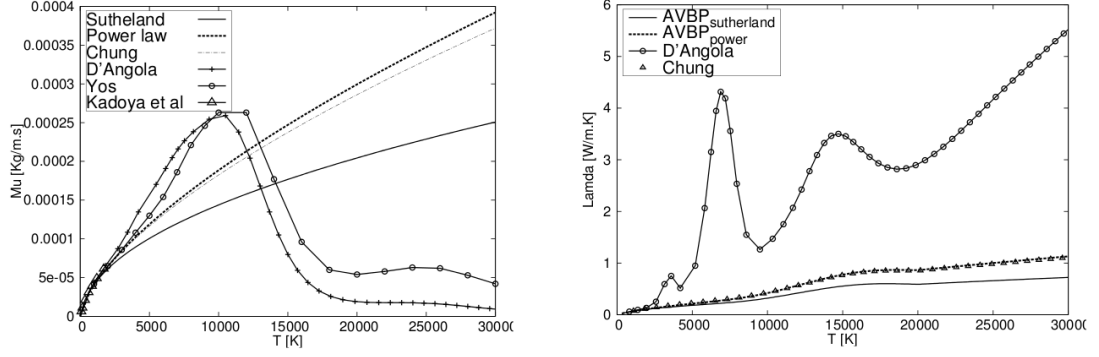


FIGURE 3.1: Dynamic viscosity (left) and thermal conductivity (right) $P = 1[atm]$ mixture AIR/CH_4 , stoichiometric ratio $\phi = 0.8$

The heat conduction coefficient of the gas mixture is computed using the molecular Prandtl number of the mixture, yielding:

$$\lambda = \frac{\mu C_p}{Pr} \quad (3.22)$$

3.2.6 Kinetics

The source terms $\dot{\omega}_k$ (reaction rate of species) and $\dot{\omega}_T$ (rate of heat release) in Eqs. 3.2 & 3.4 are related to combustion. In AVBP these terms are computed from Arrhenius laws for N reactants $\mu_{k,j}$ and for M reactions as:

$$\sum_{k=1}^N \nu'_{k,j} \mu_{k,j} \rightleftharpoons \sum_{k=1}^N \nu''_{k,j} \mu_{k,j} \quad (3.23)$$

The reaction rate of species is then the sum of rates $\dot{\omega}_{k,j}$ produced by each reaction:

$$\dot{\omega}_k = \sum_{j=1}^M \dot{\omega}_{k,j} = W_k \sum_{j=1}^M \nu_{k,j} Q_j, \quad (3.24)$$

where $\nu_{k,j} = \nu''_{k,j} - \nu'_{k,j}$ and Q_j is the rate of progress of reaction j , it is expressed as:

$$Q_j = K_{f,j} \prod_{k=1}^N \left(\frac{\rho Y_k}{W_k} \right)^{\nu'_{k,j}} - K_{r,j} \prod_{k=1}^N \left(\frac{\rho Y_k}{W_k} \right)^{\nu''_{k,j}} \quad (3.25)$$

In Eq. 3.25 $K_{f,j}$ and $K_{r,j}$ are the forward and reverse rates of reaction. They are computed as:

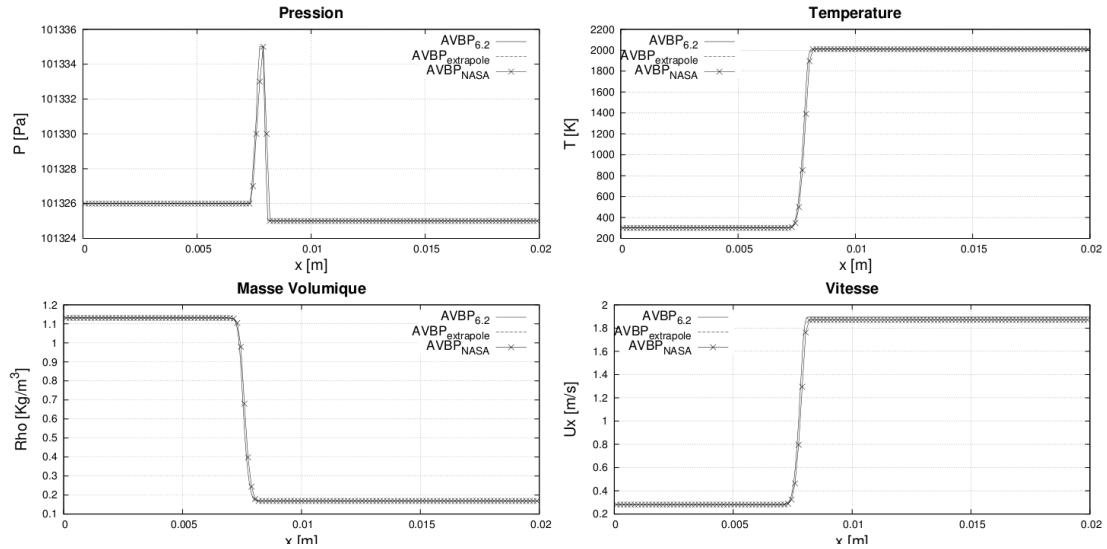


FIGURE 3.2: Comparison between CM2 and LU mechanism for a 1D flame for CH_4/AIR at $\phi = 0.8$

$$K_{f,j} = A_{f,j} \exp\left(-\frac{E_{a,j}}{RT}\right), \quad (3.26)$$

and

$$K_{r,j} = \frac{K_{f,j}}{K_{eq}} \quad (3.27)$$

K_{eq} (equilibrium constant) is defined in AVBP as in Kuo [?]:

$$K_{eq} = \left(\frac{p_0}{RT}\right)^{\sum_{k=1}^N \nu_{kj}} \exp\left(\frac{\Delta S_j^0}{R} - \frac{\Delta H_j^0}{RT}\right) \quad (3.28)$$

Finally the heat release is calculated as in Eq.3.29 where $\Delta h_{f,k}^0$ is the mass enthalpy of formation of species k at the reference temperature $T_0 = 0[K]$.

$$\dot{\omega}_T = - \sum_{k=1}^N \dot{\omega}_k \Delta h_{f,k}^0 \quad (3.29)$$

In order to account for phenomena such as dissociation or recombination, another task of CERFACS in the FAMAC project was to test a more robust chemical kinetic mechanism. Figure 3.2 shows a comparison between two chemical kinetic mechanisms for a CH_4/AIR mixture: the CM2 reduced mechanisms and the analytically reduced scheme from Lu [23]. The Lu mechanism takes into account 73 reactions and 13 species. It is observed that the temperature and the flame speed present some small differences, but the analytical scheme can be considered to be valid.

Chapter 4

DNS of 2D spark plug ignition

In this chapter the coupling between a Fluent magneto-hydrodynamics (MHD) non reactive simulation of the breakdown phase and a reactive DNS was performed. The geometry and initial conditions were obtained from an experiment at the CORIA laboratory. It corresponds to a nanosecond spark system called the Nsec spark. The aim of this exercise was to account for the plasma magnetic effects at the initial stages of the ignition process. An AVBP non reactive simulation was first performed, starting from an instantaneous solution of the Fluent (MHD) simulation. Various initial solutions were tested, to see until when it is important to account for the plasma physics after the spark discharge. Then, reactive simulations initialized again with different instantaneous Fluent solutions were performed, to observe the different flame kernel developments.

4.1 Set up and coupling

4.1.1 FLUENT (MHD) and AVBP coupling

One of the task of CERFACS in the FAMAC project is the coupling of the plasma and combustion models. The choice made by CERFCAS is to use an instant solution from the Fluent MHD simulation to initialize the combustion calculation. It is important to remember that developing a model that takes into account both the physics of plasma and of the combustion would be really complex and out of scope of the present work.

The first task to be performed was to convert the instantaneous MHD solutions, initially in FLUENT format, into the AVBP format. Figure 4.1 shows the process to convert an instantaneous solution from FLEUNT to AVBP (H5). To begin with the fields of the FLUENT simulations are recovered in the form of the primitive variables P , T , u , v ,

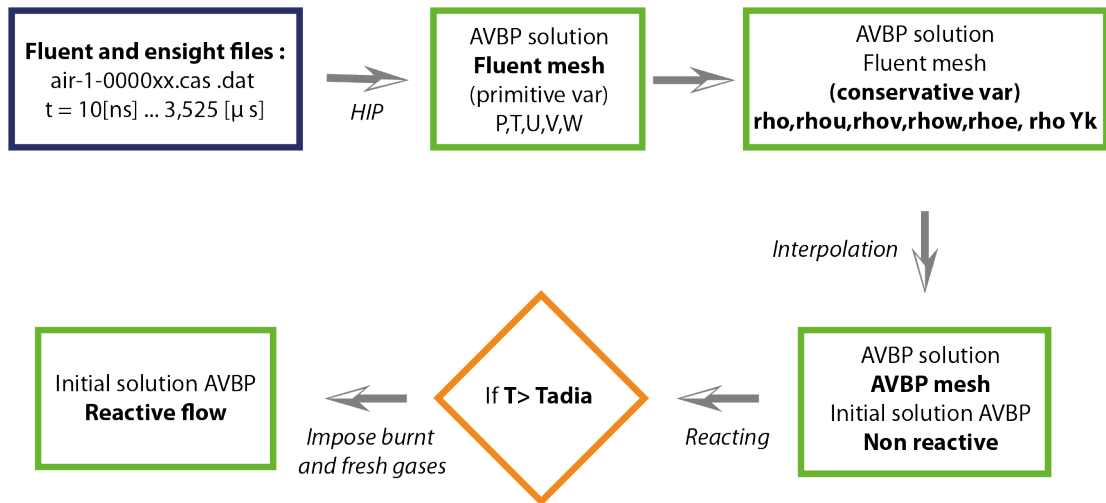


FIGURE 4.1: Flow diagram of conversion process, FLUENT format to AVBP

ρ . This step is performed by HIP which is a package from CERFACS for manipulating unstructured computational grids. Once the primitive variables fields are retrieved in H5 format the next step is to calculate the conservative variables that AVBP uses: ρ , ρe , ρu , ρv , ρY_k . At this point the total energy e is calculated as presented in Chapter 3. Consequently the instantaneous solutions are then interpolated to a new AVBP mesh in order to have a better resolution in the regions far from the electrodes. At this point the interpolated solution can be use to start a non reactive simulation with air. In order to start a reactive calculation, air is replaced by burnt and fresh gases following a temperature criterion: if the temperature T is higher than the adiabatic flame temperature T_{adia} gases are burnt, otherwise they are fresh gases.

Figures [4.2- 4.4] show the pressure, temperature, density and velocity fields for both the AVBP and the FLUENT formats. Variables are plotted along the central axis.

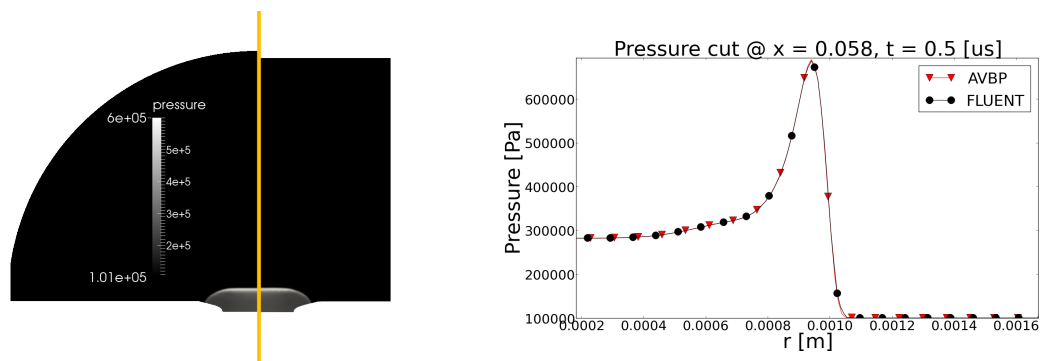


FIGURE 4.2: Pressure Fields [Pa]. Left side: AVBP format, Right side: FLUENT format

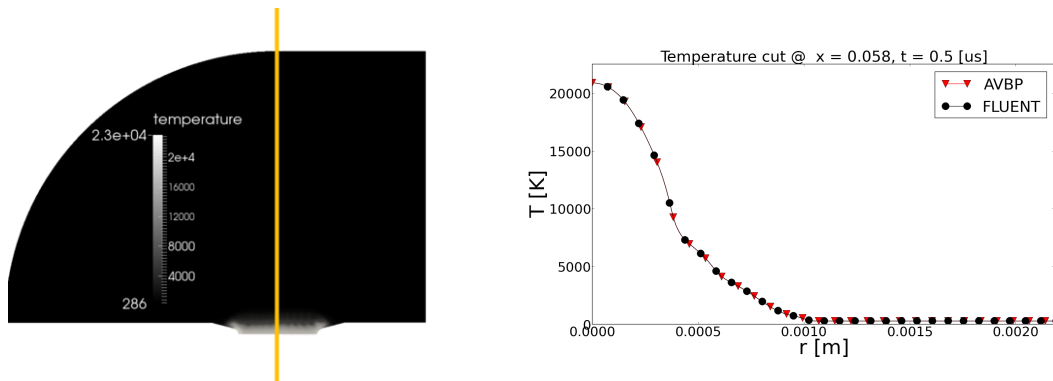


FIGURE 4.3: Temperature Fields [K]. Left side: AVBP format, Right side: FLUENT format

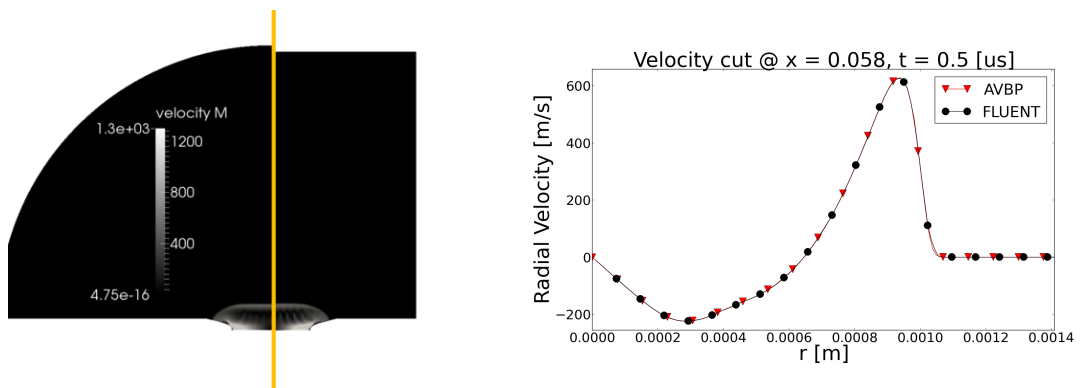


FIGURE 4.4: Velocity Fields [$\frac{m}{s}$]. Left side: AVBP format, Right side: FLUENT format

AVBP	FLUENT
<ul style="list-style-type: none"> • Conservative equations of reacting flows • Mass, energy, momentum and species equations • Species: AIR 	<ul style="list-style-type: none"> • Navier-Stokes coupled with Maxwell's equations • Fluid: Mass conservation, energy, momentum equations • Electrical: Scalar potential and Vector Potential • Species: AIR

TABLE 4.1: Equations solved in the MHD simulation

4.1.2 FLUENT (MHD) and AVBP simulations

For the sake of understanding the set up of both simulations are presented together. The FLUENT simulation is based on the work of [24], with the assumptions of Thermodynamic Local Equilibrium, laminar flow and negligible energy losses at the electrodes. Table 4.1 compares the numerical methodology of FLUENT and AVBP.

In MHD, the resolution of the scalar potential allows to estimate a current density, used as a component of the source terms in the momentum and energy equations. This leads to a strong coupling, with source terms of the form $j_r B_\theta$ where: j_r is the current density and B_θ is the magnetic field.

The initial conditions of the simulations are based on the measurements from the Nsec spark experiment at Coria laboratory and the physical time taken to initialize the simulation is $t = 10[ns]$. Figure 4.5 shows the initial condition for the FLUENT MHD simulation. It consists of a rectangular channel between both electrodes. The channel has a uniform pressure and temperature of $P = 65[bar]$, $T = 45000[K]$, and has a radius of $r = 150[\mu m]$. At the exterior of the channel atmospheric conditions for the pressure and temperature, $P = 101325.0[Pa]$ and, $T = 297[K]$ are used. The total energy deposit into the model is $E = 9.6[mJ]$

Both AVBP and FLUENT simulations are 2D axy-symmetric. Figure 4.6 shows the mesh for both simulations. The FLUENT mesh has 205648 nodes, 204676 cells (quads) with a minimum size of $2[\mu m]$. The AVBP mesh has 224454 nodes, 447228 cells (triangles) and a minimum cell size of $h_{min} = 5[\mu m]$.

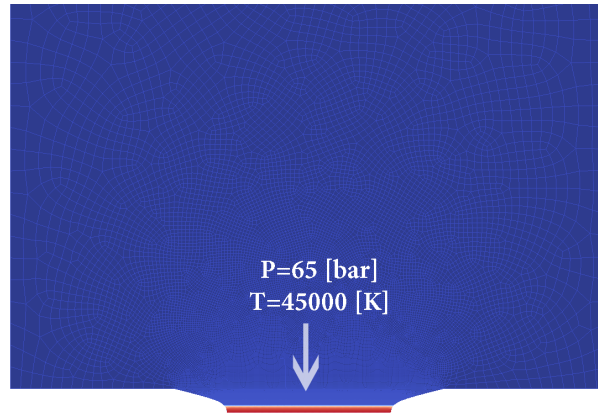


FIGURE 4.5: Initial and boundary conditions for the FLUENT MHD simulation

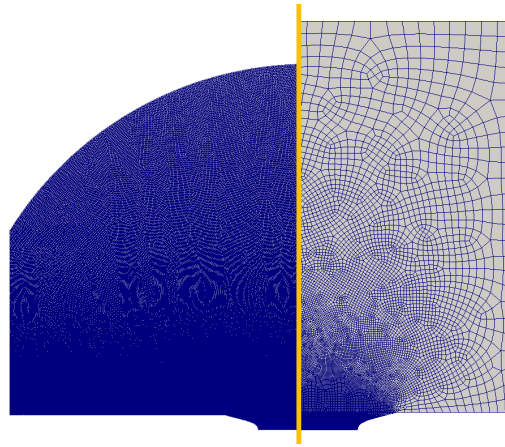


FIGURE 4.6: Left: AVBP mesh, Right:FLUENT mesh.

Figure 4.7 shows the boundary conditions used in both simulations. Heat losses in the electrodes were not taken into account hence, an adiabatic no slip wall condition was used on the electrodes. The 3[mm] electrode gap was treated as symmetry. Finally for the AVBP simulation an outlet pressure boundary condition was used at the border of the computational domain with a constant value of $P = 101325.0[Pa]$. This type of boundary condition was defined as NSCBC in order to avoid acoustic reflexion on the boundary. The boundary conditions for the FLUENT solution were implemented in a similar way as in [25] where the current and scalar potential are imposed at the cathode.

4.2 Non reactive simulations

A non reactive simulation was first performed in order to validate the process of converting the FLUENT instantaneous solution to the AVBP (H5) format. The computation

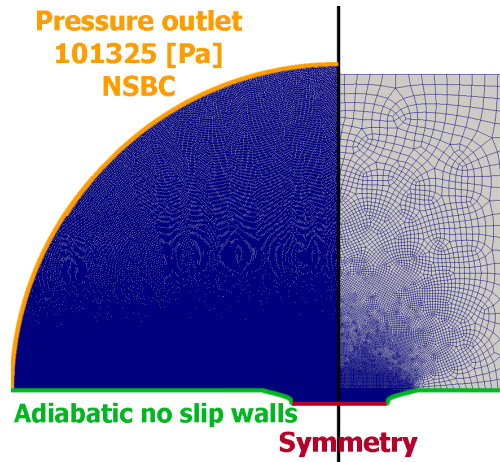


FIGURE 4.7: Boundary conditions. Left: AVBP simulation, Right: FLUENT simulation.

was initialized with the FLUENT instantaneous solution corresponding to $t_{init} = 0.05\mu s$. Figure 4.8 shows a diagram to visualize the methodology.

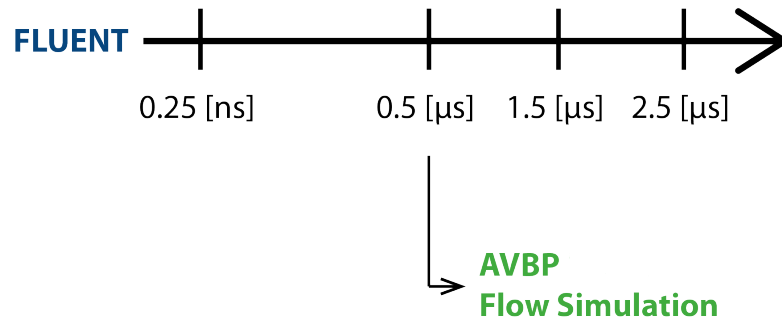


FIGURE 4.8: Methodology to initialize AVBP from a FLUENT instantaneous solution at $t_{init} = 0.05\mu s$

Table 4.2 present the numerical schemes used in both simulations. Other numerical aspects are mentioned for AVBP, that refer to the pressure shock handling and the artificial viscosity.

AVBP numerics	FLUENT numerics
TTGC, explicit scheme 3 th order in space and time	Implicit scheme, upwind 2 nd order spatial integration
Artificial viscosity sensor activated Shock model: Cook, A.W. & Cabot, W.H	Not specified

TABLE 4.2: Numerical schemes for both simulations

Tables [4.3- 4.5] show a qualitative comparison of the pressure, temperature and velocity fields at three different instants: $t = 1.525[\mu s]$ $t = 2.525[\mu s]$ $t = 3.525[\mu s]$. A

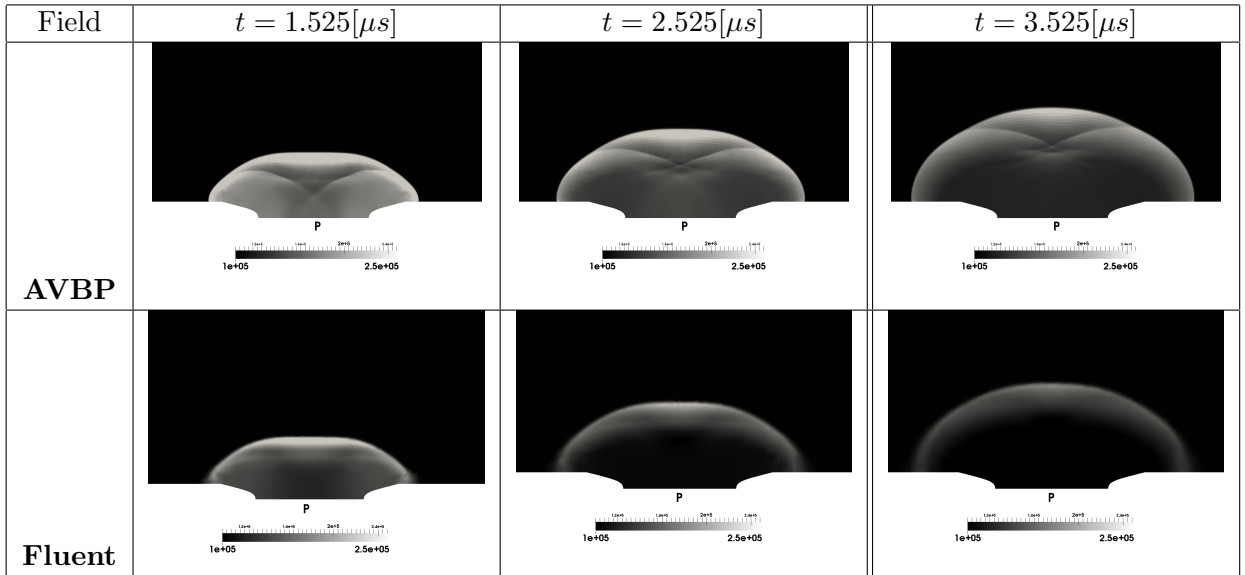


TABLE 4.3: Pressure [Pa] fields for both FLUENT and AVBP simulations.

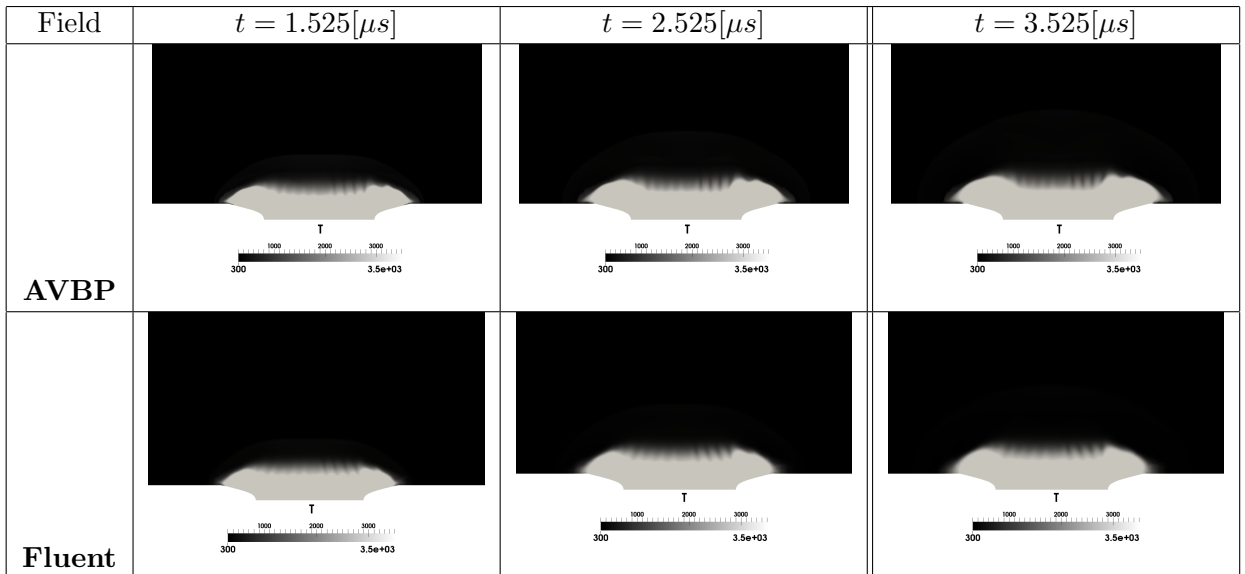


TABLE 4.4: Temperature [K] fields for both FLUENT and AVBP simulations.

better resolution is observed in the AVBP fields thanks to the mesh and the third-order numerical scheme. In general the behavior is quite similar in both simulations. In the pressure fields a pair of second pressure waves that intersect in the center is observed with AVBP. For the velocity and temperature fields a strange pattern is present in both simulations in the form of "strides or marks", probably due to numerical difficulties in the FLUENT simulations and persistent in the AVBP calculations.

Table 4.4 shows the temperature field evolution. A similar profile is observed for the three instants shown. It is important to remember that the electrodes were considered

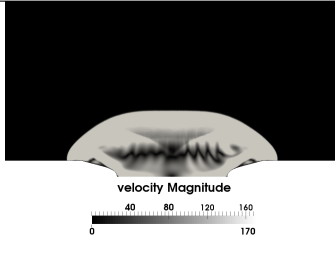
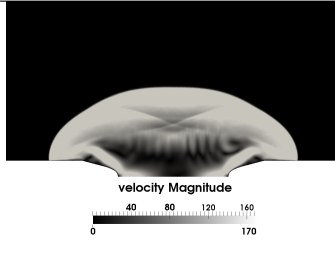
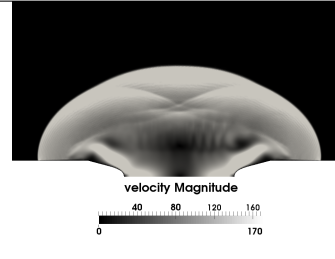
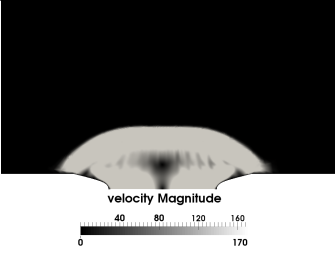
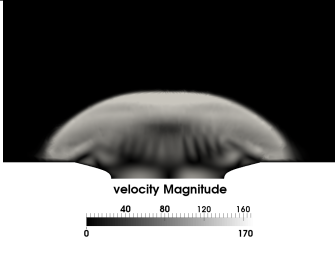
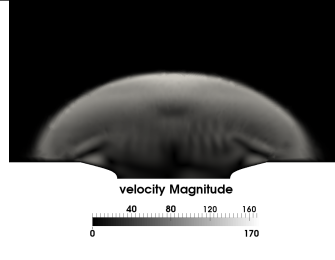
Field	$t = 1.525[\mu s]$	$t = 2.525[\mu s]$	$t = 3.525[\mu s]$
AVBP			
Fluent			

TABLE 4.5: Velocity (magnitude) [$\frac{m}{s}$] fields for both FLUENT and AVBP simulations.

adiabatic. If conduction losses were taken into account, as it is in reality, they would affect the temperature profiles and less energy would be available for ignition.

For the sake of simplicity results are presented over a line cut in the computational domain as shown in Figure 4.9. Results are compared with the experiments and the FLUENT simulation.

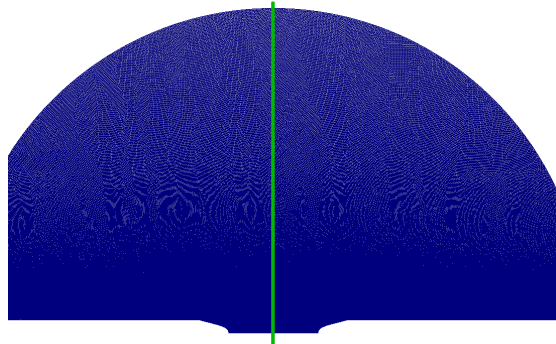


FIGURE 4.9: Cut position $x = 0.00548[mm]$

In order to compare the development of the shock wave, shown in Figure 4.10, the location of the peak value of pressure is considered at each instantaneous solution. The experimental results were measured in the N-spark configuration. The pressure wave with AVBP expands faster than with FLUENT, possibly due to the numerical scheme. Both codes are in reasonable agreement with the experiment.

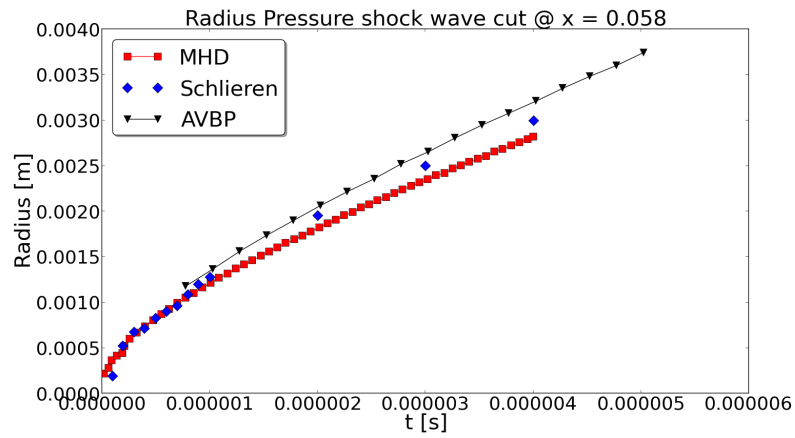


FIGURE 4.10: Shock wave speed plotted over the line $x = 0.00548[m]$. AVBP: black triangles, Experiments: blue diamonds, FLUENT: red squares.

Comparison of the temperature is done at three different points: near the cathode $x = 0.00448[m]$, in the middle plane $x = 0.00548[m]$ and near the anode, $x = 0.00648[m]$. Figures [?? - ??] show the three comparisons. Good agreement is observed, although no experimental data was available in the middle plane.

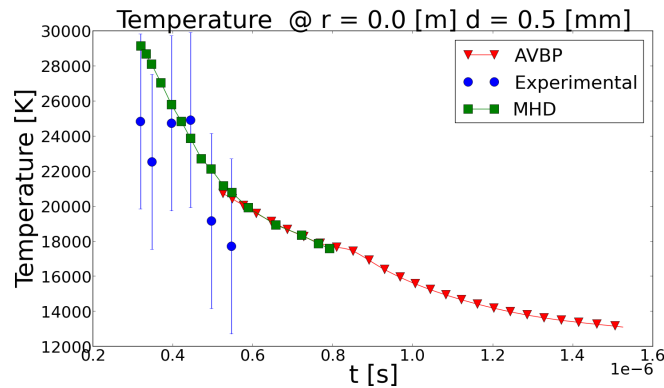


FIGURE 4.11: Experimental, FLUENT and AVBP data $t_{init} = 0.525[\mu s]$

Figure 4.15 shows a comparison between the Schlieren and the numerical result of AVBP (density gradient) at $t = 30[\mu s]$. The shock wave shape is quite different, and the timing of both the simulation and the experient should be double-checked (which is in progress). Wrinkles introduced by the FLUENT initial field are still visible at the central zone.

A closer look to the pressure, temperature and velocity signals in the middle plane at $x = 0.00548[m]$ is presented in Figures [4.15 - 4.17]. Results from AVBP are compared to the FLUENT simulations. The pressure and velocity signals contain some oscillation in the AVBP data, due to strong gradients and higher peak values. The behavior of

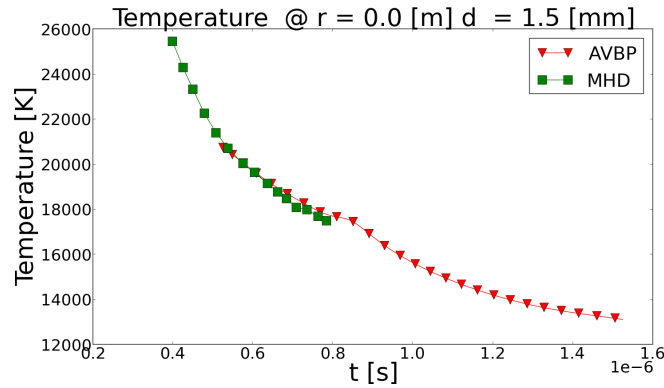


FIGURE 4.12: FLUENT and AVBP data, $t_{init} = 0.525[\mu s]$ (No experimental data available)

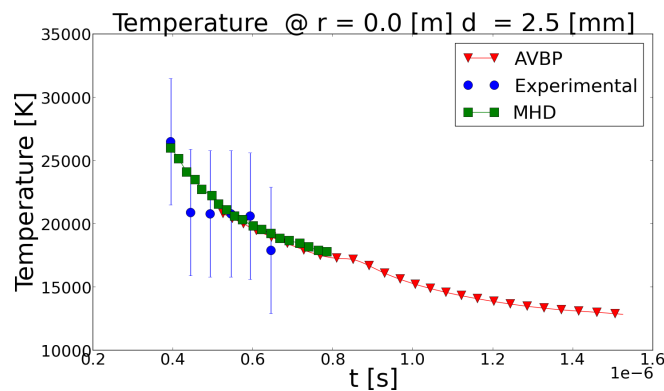


FIGURE 4.13: Experimental, FLUENT and AVBP data, $t_{init} = 0.525[\mu s]$

the temperature is almost the same in shape and really close in magnitude for both simulations (AVBP and FLUENT) as shown in Figure 4.16.

Table 4.6 shows that the second pressure wave in the AVBP results could be due to a geometrical effect of the small angle of the cathode. The images shown are computed as follows: $\frac{|grad(\rho)|}{\rho}$, and show the pressure wave evolution. This second pressure wave was already observed by [12] and in the work of Maestro et.al. [11]. The reason for this second pressure wave seems to be also a geometry expansion effect in this case (Figure 4.18).

In conclusion, a good behavior of the code was observed and results were validated against the few experimental data that were available. AVBP captured a similar phenomena as the FLUENT, starting from the instantaneous solution at $t_{init} = 0.5[\mu s]$. The use of the Fluent (MHD) simulations appears therefore to be not really worthy after this time.

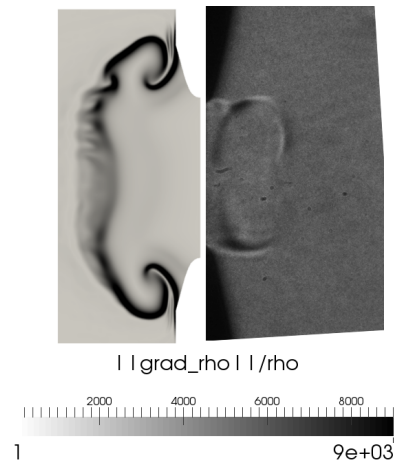


FIGURE 4.14: Experimental and AVBP screen shots at $t = 30[\mu s]$ AVBP results computed as: $\frac{|grad(\rho)|}{\rho}$

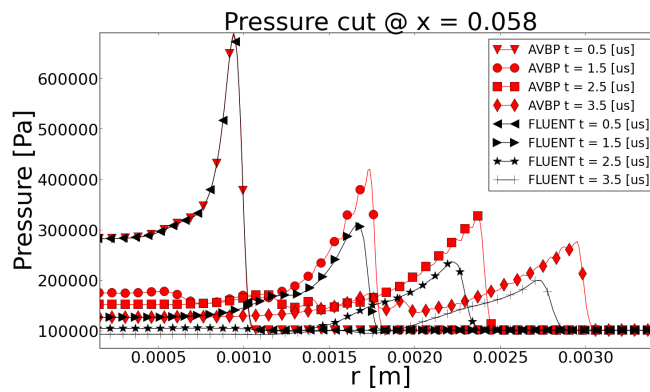


FIGURE 4.15: Pressure evolution at $x = 0.00548[m]$ for the FLUENT and AVBP calculations

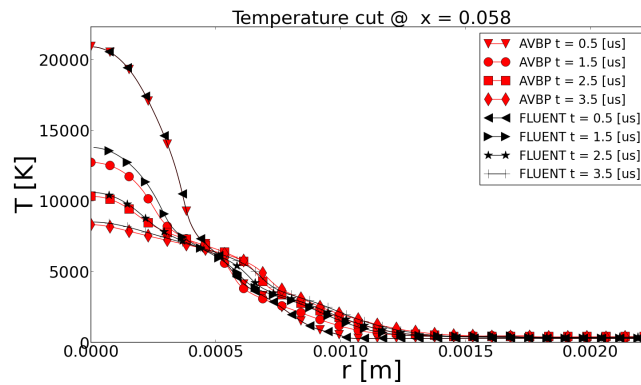


FIGURE 4.16: Temperature at $x = 0.00548[m]$ for the FLUENT and AVBP calculations

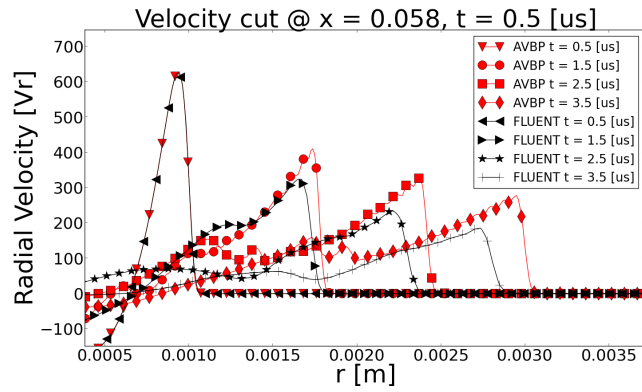


FIGURE 4.17: Velocity at $x = 0.00548[m]$ for the FLUENT and AVBP calculations

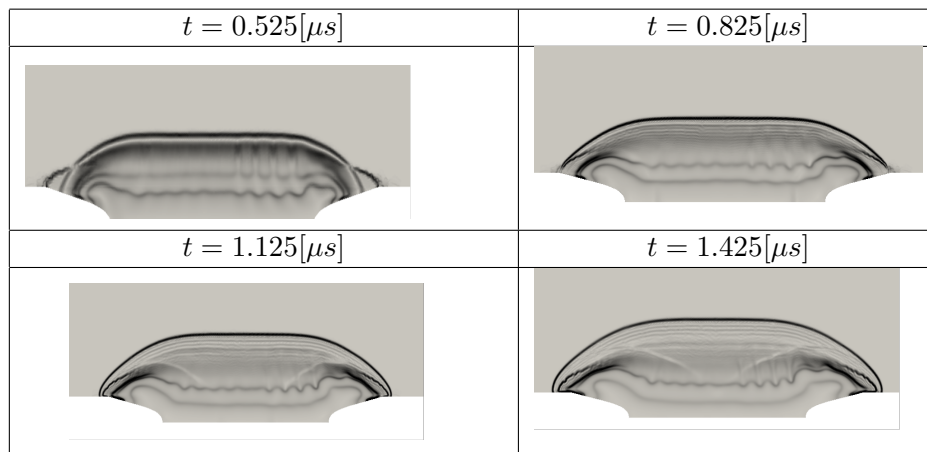


TABLE 4.6: Shock wave evolution, early stages of the time evolution.

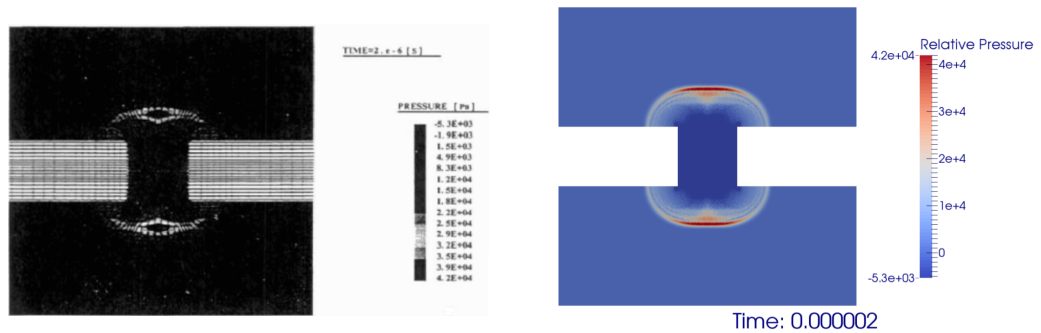
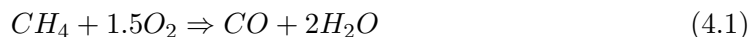


FIGURE 4.18: Second pressure wave found previously in the literature: [12], [11]

4.3 Reactive simulations

As it was previously mentioned, the main task of CERFACS within the FAMAC project is to couple a plasma model with combustion in order to link the magnetic field and plasma effects to the initiation of combustion. The set up of this AVBP reactive simulations is exactly the same as the previous non reactive cases. It now includes a 2-step chemical scheme (CM2) with 5 species and 2 reactions:



In order to initiate combustion, the FLUENT solution used as initial solution was modified: air was replaced by burnt gases where $T > T_{adia} = 2212.3[K]$, T_{adia} being the adiabatic temperature of a stoichiometric mixture CH_4/AIR at atmospheric conditions, and by fresh gases elsewhere. Three different instantaneous solutions from the FLUENT simulation were chosen: $t_{init} = 0.525[\mu s]$, $t_{init} = 1.525[\mu s]$, $t_{init} = 2.525[\mu s]$ in order to test different instants to initiate the combustion (Figure 4.3).

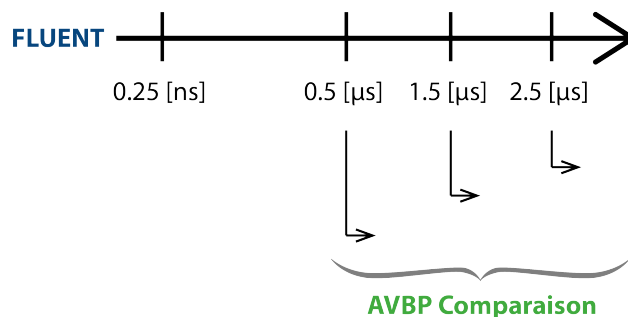


FIGURE 4.19: Methodology for the three reactive simulations starting from: $t_{init} = 0.525[\mu s]$, $t_{init} = 1.525[\mu s]$ and $t_{init} = 2.525[\mu s]$

Figure 4.20 shows the three instants, the isoline in red represents $T = 2212.3[K]$, illustrating the hot gas zone. In the same way as in the non reactive cases, the initial solution present some numerical noise that comes from the FLUENT simulation.

Figure 4.21 shows the Flame Front development in the line $x = 0.00548[m]$. In order to calculate the evolution of the flame front, the reference value was taken at the maximum value of heat release. The evolution of the flame in the simulation started at $t_{init} = 0.525[\mu s]$ is much faster than the other two simulations initialized at later times $t_{init} =$

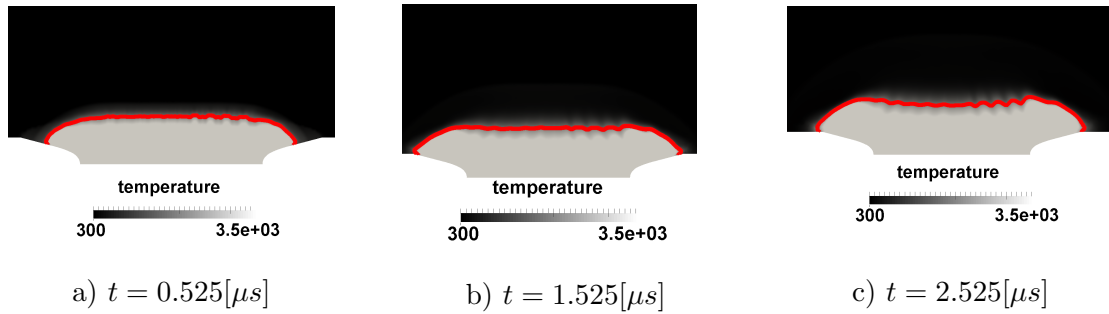


FIGURE 4.20: Temperature fields: isoline $T = 2212.3[K]$ for three different Fluent instantaneous solutions:

$1.525[\mu s]$ and $t_{init} = 2.525[\mu s]$. This may be due to the temperature profile much hotter for the $t_{init} = 0.525[\mu s]$ as shown in Figure 4.22

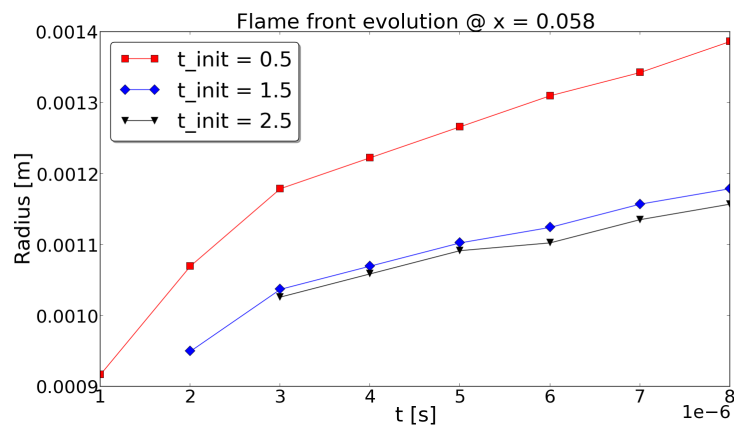


FIGURE 4.21: Flame front development in time at the line $x = 0.00548[m]$ for the three simulations $t_{init} = 0.525[\mu s]$, $t_{init} = 1.525[\mu s]$, $t_{init} = 2.525[\mu s]$

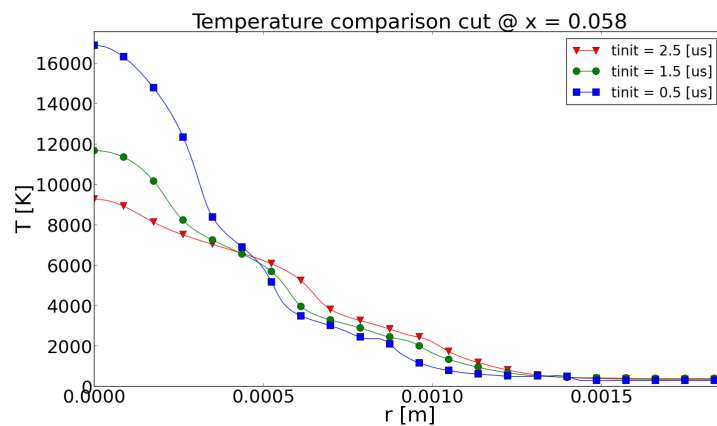


FIGURE 4.22: Temperature profiles at the line $x = 0.00548[m]$ for the three simulations $t_{init} = 0.525[\mu s]$, $t_{init} = 1.525[\mu s]$, $t_{init} = 2.525[\mu s]$

Tables [4.7- 4.8] present the time evolution of the pressure shock wave and the flame front development. It is observed that the flame front and the shock wave propagate faster for earlier initializations. The lower dissipation of the numerical scheme used in

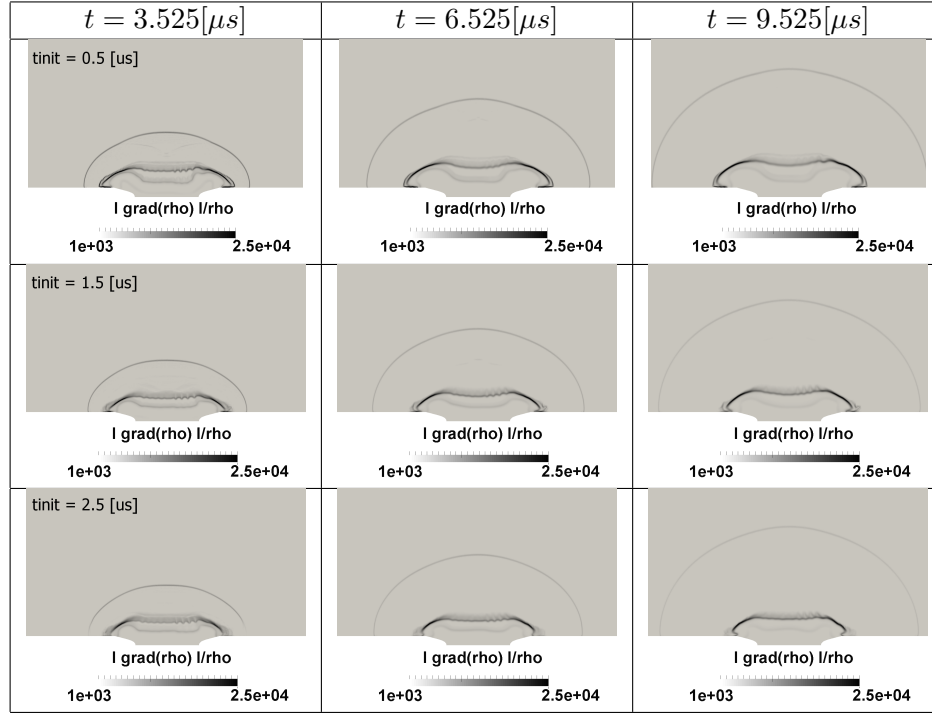


TABLE 4.7: Evolution of the pressure wave and the flame: $\frac{|grad(\rho)|}{\rho}$

AVBP is again certainly the cause of this effect.

The importance of the instantaneous FLUENT MHD solution chosen to start the AVBP reacting simulation is illustrated in Table 4.8. It is observed at $t = 9.525[\mu s]$ that the surface of burnt gases is larger for $t_{init} = 0.525[\mu s]$. This observation is confirmed in Figure 4.23 where the heat release advances faster for $t_{init} = 0.525[\mu s]$. A comparison with experimental results needs to be done in order to conclude about the best initial solution to start the combustion calculation.

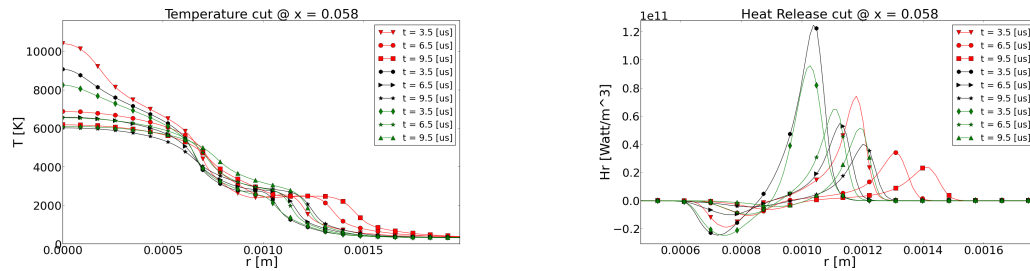


FIGURE 4.23: Temperature $[K]$ (left) and Heat release $[\frac{Watt}{m^3}]$ (right). Red lines: Initial solution $t = 0.525[\mu s]$, Black lines: $t = 1.525[\mu s]$, Green lines $t = 3.525[\mu s]$

Figure 4.25 shows that the three simulations well resolve the flame front, with no undershoot or overshoot on the density profile. From Figure 4.24, it appears that the

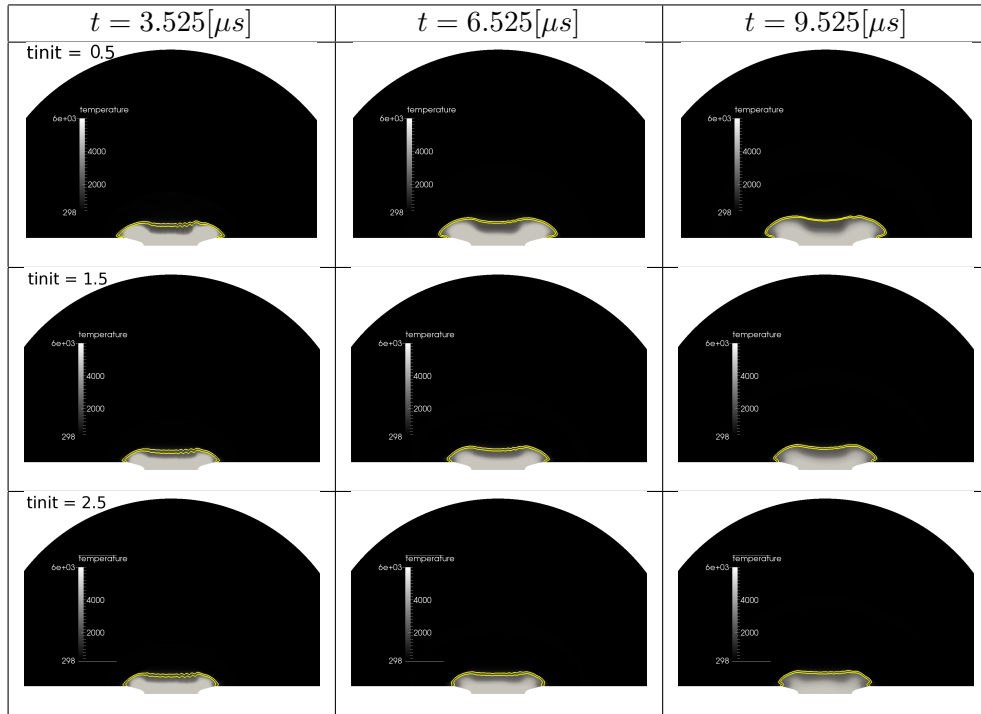


TABLE 4.8: Temperature fields, Isoline $Heatrelease = 2 \times 10^9 [Watt/m^3]$

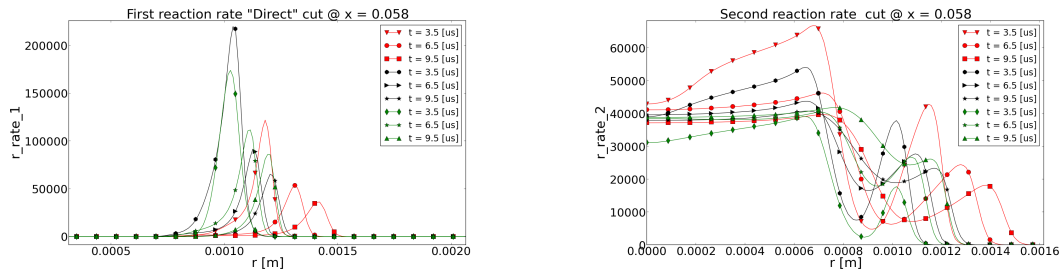


FIGURE 4.24: Reaction rate 1 (left) $CH_4 + 1.5O_2 \Rightarrow CO + 2H_2O$ and 2 (right) $CO + 0.5O_2 \Leftrightarrow CO_2$. Red lines: Initial solution $t = 0.525[\mu s]$, Black lines: $t = 1.525[\mu s]$, Green lines $t = 3.525[\mu s]$

direct reaction takes place as expected and that the second reaction takes it maximum values within the burnt gases.

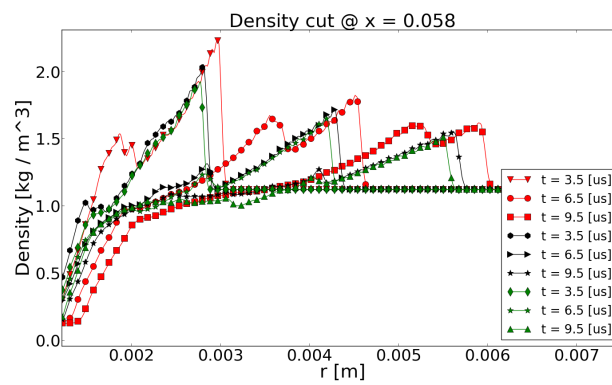


FIGURE 4.25: Density $[\frac{Kg}{m^3}]$. Red lines: Initial solution $t = 0.525[\mu s]$, Black lines: $t = 1.525[\mu s]$, Green lines $t = 3.525[\mu s]$

Chapter 5

Conclusions

A strategy to transfer the FLUENT files to AVBP format was developed. This change of format was performed in order to initialize AVBP with a non reactive solution obtained with FLUENT MHD, and to compare the reacting non-MHD simulation of AVBP with the non-reacting, MHD simulation of FLUENT. The objective was to evaluate the importance of MHD in the process of ignition.

A non reactive AVBP simulation starting from $t_{init} = 0.525[\mu s]$ proved to give similar results as FLUENT (MHD). Less dissipation was observed with AVBP because of the centered high order schemes, but oscillations appeared due to strong gradients. AVBP captured well the shock wave propagation, and a second pressure wave appeared due to geometrical effects. To achieve the evaluation of the role of MHD, a simulation with AVBP starting from $t = 0s$ is in progress.

In a second step, reactive simulations with AIR/CH_4 mixture were performed, initialized with three different instantaneous MHD solutions from FLUENT. It was observed that the sooner the combustion is activated, the faster the flame front propagates. It is important to note that the initial shape of the flame kernel is determined by the temperature threshold used to introduce hot gases. Work is still in progress with a reactive simulation with a AIR/C_3H_8 mixture, in order to compare with the experiment of CO-RIA.

Bibliography

- [1] European Parliament and Council of the European Union. REGULATION (EU) No 333/2014 OF THE EUROPEAN PARLIAMENT AND OF THE COUNCIL of 11 March 2014 amending Regulation (EC) No 443/2009 to define the modalities for reaching the 2020 target to reduce CO₂ emissions from new passenger cars THE. *Official Journal of the European Union*, (333):15–21, 2014.
- [2] S M Shahed and Karl-Heinz Bauer. Parametric Studies of the Impact of Turbocharging on Gasoline Engine Downsizing, 2009. URL <http://dx.doi.org/10.4271/2009-01-1472>.
- [3] Bryce C. Thelen, Daekeun Chun, Elisa Toulson, and Tonghun Lee. A study of an energetically enhanced plasma ignition system for internal combustion engines. *IEEE Transactions on Plasma Science*, 41(12):3223–3232, 2013. ISSN 00933813. doi: 10.1109/TPS.2013.2288204.
- [4] Charles D. Cathey, Tao Tang, Taisuke Shiraishi, Urushihara Urushihara, András Kuthi, and Martin A. Gundersen. Nanosecond plasma ignition for improved performance of an internal combustion engine. *IEEE Transactions on Plasma Science*, 35(6 PART 1):1664–1668, 2007. ISSN 00933813. doi: 10.1109/TPS.2007.907901.
- [5] Neil Fraser, Hugh Blaxill, Grant Lumsden, and Mike Bassett. Challenges for Increased Efficiency through Gasoline Engine Downsizing, 2009. ISSN 1946-3944. URL <http://dx.doi.org/10.4271/2009-01-1053>.
- [6] Maren Thiele, Stefan Selle, Uwe Riedel, Jürgen Warnatz, and Ulrich Maas. Numerical simulation of spark ignition including ionization. In *Proceedings of the Combustion Institute*, volume 28, pages 1177–1185, 2000. doi: 10.1016/S0082-0784(00)80328-8.
- [7] T Kravchik and E Sher. Numerical modeling of spark-ignition and flame initiation in a quiescent methane-air mixture. *Combust. and Flame*, 99(August):635–643, 1994.

- [8] Rudolf Maly. Ignition model for spark discharges and the early phase of flame front growth. *Symposium (International) on Combustion*, 18(1):1747–1754, 1981. ISSN 00820784. doi: 10.1016/S0082-0784(81)80179-8.
- [9] D Bradley and F K K Lung. Spark ignition and the early stages of turbulent flame propagation. *Combustion and Flame*, 69(1):71–93, 1987. URL <http://www.sciencedirect.com/science/article/pii/0010218087900228>.
- [10] C'esar Becerril. Étude des systèmes d ' allumage : De l ' étincelle à la flamme Table des matières. 2013.
- [11] Dario Maestro. Ignition Fundamentals for Internal Combustion Engines. 2014.
- [12] T. Kravchik, E. Sher, and J. B. Heywood. From Spark Ignition to Flame Initiation. *Combustion Science and Technology*, 108(1-3):1–30, 1995. ISSN 0010-2202. doi: 10.1080/00102209508960387.
- [13] Stefan Pischinger and John B. Heywood. A model for flame kernel development in a spark-ignition engine. *Symposium (International) on Combustion*, 23(1):1033–1040, 1991. ISSN 00820784. doi: 10.1016/S0082-0784(06)80361-9.
- [14] O. Colin and K. Truffin. A spark ignition model for large eddy simulation based on an FSD transport equation (ISSIM-LES). *Proceedings of the Combustion Institute*, 33(2):3097–3104, 2011. ISSN 15407489. doi: 10.1016/j.proci.2010.07.023.
- [15] I. N. Kosarev, N. L. Aleksandrov, S. V. Kindysheva, S. M. Starikovskaia, and a. Yu Starikovskii. Kinetics of ignition of saturated hydrocarbons by nonequilibrium plasma: C₂H₆- to C₅H₁₂-containing mixtures. *Combustion and Flame*, 156(1):221–233, 2009. ISSN 00102180. doi: 10.1016/j.combustflame.2008.07.013. URL <http://dx.doi.org/10.1016/j.combustflame.2008.07.013>.
- [16] G. Taylor. The Formation of a Blast Wave by a Very Intense Explosion. II. The Atomic Explosion of 1945. *Proceedings of the Royal Society A: Mathematical, Physical and Engineering Sciences*, 201(1065):175–186, 1950. ISSN 1364-5021. doi: 10.1098/rspa.1950.0050.
- [17] I. N. Kosarev, N. L. Aleksandrov, S. V. Kindysheva, S. M. Starikovskaia, and a. Yu Starikovskii. Kinetics of ignition of saturated hydrocarbons by nonequilibrium plasma: CH₄-containing mixtures. *Combustion and Flame*, 154(3):569–586, 2008. ISSN 00102180. doi: 10.1016/j.combustflame.2008.03.007.
- [18] G Hagelaar and L Pitchford. Solving the Boltzmann equation to obtain electron transport coefficients and rate coefficients for *Plasma Sources Science and Technology*, 14(4):722–733, 2005. ISSN 0963-0252. doi: 10.1088/0963-0252/14/

- 4/011. URL http://www.iop.org/EJ/article/0963-0252/14/4/011/psst5_4_011.pdf.
- [19] Thierry Poinsoot and Denis Veynante. Theoretical and Numerical Combustion. *Combustion and Flame*, 32(1):534, 2005. ISSN 00102180. doi: 686310.1016/j.combustflame.2007.07.002S0010-2180(07)00176-9. URL http://books.google.com/books?hl=en&lr=&id=cqFDkeVABYoC&oi=fnd&pg=PR11&dq=Theoretical+and+numerical+combustion&ots=LbrXMPH_hD&sig=bKfKFeR6PECG5IKfBY1ifRbMM7c.
- [20] Sanford Gordon and B.J. McBride. Thermodynamic Data to 20 000 K for Monatomic Gases. *NASA Technical Report No. TP-1999-208523*, (June), 1999. URL <http://scholar.google.com/scholar?hl=en&btnG=Search&q=intitle:Thermodynamic+Data+to+20+000+K+for+Monatomic+Gases#0>.
- [21] Michael J. Zehe, Sanford Gordon, and Bonnie J. McBride. CAP: A Computer Code for Generating Tabular Thermodynamic Functions from NASA Lewis Coefficients. (February), 2002.
- [22] Gas-phase Chemical. A software package for the analysis of gas-phase chemical and plasma kinetics. *Design*, 49(September):1–181, 2000. URL <http://www.ncbi.nlm.nih.gov/pubmed/21821594>.
- [23] Tianfeng Lu and Chung K. Law. A criterion based on computational singular perturbation for the identification of quasi steady state species: A reduced mechanism for methane oxidation with NO chemistry. *Combustion and Flame*, 154(4):761–774, 2008. ISSN 00102180. doi: 10.1016/j.combustflame.2008.04.025.
- [24] P Freton, J J Gonzalez, and A Gleizes. Comparison between a two- and a three-dimensional arc plasma configuration, 2000. ISSN 0022-3727.
- [25] P Freton, J J Gonzalez, M Masquère, and Frank Reichert. Magnetic field approaches in dc thermal plasma modelling. *Journal of Physics D: Applied Physics*, 44(34):345202, 2011. URL <http://stacks.iop.org/0022-3727/44/i=34/a=345202>.